Thermodynamic and Superstatistical Analysis of a Harmonic Oscillator with Position-Dependent Mass

Abstract

In this paper, we investigate the thermodynamic behavior of a quantum harmonic oscillator with a position-dependent mass (PDM), where spatial inhomogeneity is introduced through a deformation parameter α. Using the exact energy spectrum, we derive the associated thermodynamic quantities and perform a superstatistical analysis by incorporating fluctuations of the inverse temperature. Within this framework, we examine how mass deformation affects the superstatistical energy distribution and the resulting modified thermodynamic responses. Our results show that increasing α leads to a reduction in entropy and specific heat, reflecting a confinement-induced decrease in the number of accessible microstates. The partition function and free energy display smooth variations across all parameter regimes, indicating the absence of critical phase transitions. Overall, this work highlights the combined effects of mass deformation and superstatistical fluctuations on the thermal behavior of the system and reveals distinctive features that differentiate the PDM oscillator from its constant-mass counterpart.

Keywords: Thermodynamic properties; Superstatistics Properties; Schrodinger equation; Harmonic oscillator; Position dependent mass.

1 Introduction

In recent decades, the study of quantum systems with position-dependent mass (PDM) has gained considerable attention due to its broad applications in condensed-matter physics, semiconductor heterostructures, quantum wells, quantum dots, and other nanoscale systems [1–11]. Such systems are essential for describing the behavior of charge carriers in non-uniform media, including He clusters, abrupt heterojunctions, superlattices, and various optoelectronic devices. From a theoretical standpoint, the PDM Schrödinger equation has been addressed through several analytical approaches, such as Darboux transformations [12], the factorization method [13], the Nikiforov–Uvarov (NU) and extended NU formalisms [14], supersymmetric quantum mechanics [15,16], and point canonical transformations [17]. Furthermore, several works have calculated the thermodynamic properties of different PDM potentials — for example, the modified Rosen–Morse potential — analyzing how temperature and the maximum quantum state influence various thermodynamic quantities.

A wide range of potential models — including the Kratzer, Pöschl–Teller, Morse, Coulomb, and Hulthén potentials — has been studied within the PDM framework to better understand the quantum behavior of particles in inhomogeneous media [18,19]. Recent advances in this field have also provided exact or approximate solutions of the PDM Schrödinger equation for both confined and unconfined systems, such as the infinite square well [1,20–28] and pseudoharmonic oscillators [29]. Khordad [30], in one of his works, examined the thermodynamic properties of triangular quantum wires, focusing on

entropy, specific heat, and internal energy. Dong et al. [31] derived exact solutions of the Schrödinger equation with an exponential-type position-dependent mass, while Amir and Iqbal [26] provided an analytical solution for a PDM particle confined in an infinite square well (ISW). Inyang et al. [32] recently computed various thermodynamic properties of the Eckart–Hellmann potential. More recently, Iqbal and Rus [33] investigated the time evolution of wave packets for a PDM particle in a one-dimensional ISW, revealing the presence of quantum revivals at different time intervals. In addition, El Nabulsi [34] introduced a novel formalism for analyzing the Schrödinger equation with position-dependent mass, with particular relevance to semiconductor applications.

Motivated by these developments, we first consider in this work a quantum system characterized by a deformed mass profile of the form

$$m(x) = \frac{m_0}{(1+\alpha x^2)^2}, \tag{1}$$

where m_0 is a constant reference mass and α is a deformation parameter that governs the spatial variation of the effective mass. This quadratic deformation extends previously studied models [35, 36] and provides a richer physical and mathematical structure. In this study, we confine the system within a one-dimensional harmonic oscillator potential and examine the resulting quantum dynamics in detail.

In the second part of this work, we conduct a detailed investigation of the thermodynamic and superstatistical properties of the harmonic oscillator with position-dependent mass (PDM) [37, 38]. Building on the exact analytical form of the energy spectrum, we derive the canonical partition function and examine how the deformation parameter influences the thermal behavior of the system. Furthermore, within the superstatistical framework, we incorporate fluctuations of the inverse temperature to evaluate their impact on the effective energy distribution. From these formulations, we compute and analyze the mean energy, specific heat, Helmholtz free energy, and entropy, highlighting how both mass deformation and temperature fluctuations jointly shape the system's thermodynamic responses [39, 40].

The paper is organized as follows. Section 2 provides a review of the solution methods for the harmonic oscillator with position-dependent mass. In Section 3, we evaluate the thermodynamic and superstatistical properties of the model based on the derived energy spectrum. Section 4 presents the numerical results and discussion. Finally, the main conclusions are summarized in Section 5.

2 Review of the Solution Methods for the Harmonic Oscillator with Position-Dependent Mass

In this section, presents a comprehensive and self-contained overview of the methodology for deriving the quantum states of a harmonic oscillator with a position-dependent mass [35, 36]. We study a quantum harmonic oscillator with a position-dependent mass (PDM), using a Hermitian form of the kinetic energy operator proposed by Mustafa and Mazharimousavi [41] and references therein. For a harmonic potential and a mass profile $m(x) = \frac{m_0}{(1+\alpha x^2)^2}$, the Schrödinger equation is transformed via a suitable change of variables and wavefunction rescaling.

The most general Hermitian kinetic Hamiltonian for a particle with position-dependent mass (PDM) $m(\hat{x})$ is given by [36]:

$$\hat{T} = \frac{1}{4}\left[m^{\alpha}(\hat{x})\hat{p}m^{\beta}\hat{p}m^{\gamma}(\hat{x}) + m^{\gamma}(\hat{x})\hat{p}m^{\beta}\hat{p}m^{\alpha}(\hat{x})\right], \tag{2}$$

where α, β and γ satisfy $\alpha + \beta + \gamma = -1$. In this study, we adopt the Mustafa and Mazharimousavi ordering [36, 41] with $\alpha = \gamma = -\frac{1}{4}$ and $\beta = -\frac{1}{2}$:

$$\hat{T} = \frac{1}{2}\frac{1}{m^{1/4}(\hat{x})}\hat{p}\frac{1}{m^{1/2}(\hat{x})}\hat{p}\frac{1}{m^{1/4}(\hat{x})}. \tag{3}$$

The full Hamiltonian becomes:

$$\hat{H} = \hat{T} + V = \frac{1}{2}\frac{1}{m^{1/4}(\hat{x})}\hat{p}\frac{1}{m^{1/2}(\hat{x})}\hat{p}\frac{1}{m^{1/4}(\hat{x})} + V(\hat{x}), \tag{4}$$

with $V(x) = \frac{1}{2}m_0\omega^2 x^2$.

The time-independent Schr"odinger equation then reads:

$$E\phi(x) = -\frac{\hbar^2}{2m_0}\sqrt[4]{\frac{m_0}{m(x)}}\frac{d}{dx}\sqrt{\frac{m_0}{m(x)}}\frac{d}{dx}\sqrt[4]{\frac{m_0}{m(x)}}\phi(x) + V(x)\phi(x). \tag{5}$$

We consider the mass profile:

$$m(x) = \frac{m_0}{(1+\alpha x^2)^2}, \quad 0 < \alpha < 1. \tag{6}$$

Using the transformation $\phi(x) = \sqrt[4]{m(x)/m_0}\psi(x)$, Eq. (5) becomes:

$$E\psi(x) = -\frac{\hbar^2}{2m_0}\left[(1+\alpha x^2)\frac{d}{dx}\right]^2\psi(x) + \frac{1}{2}m_0\omega^2x^2\psi(x). \tag{7}$$

Introducing the variable change:

$$q = \arctan(x\sqrt{\alpha}), \tag{8}$$

which maps $x \in (-\infty, \infty)$ to $q \in (-\frac{\pi}{2}, \frac{\pi}{2})$, we obtain:

$$\frac{d^2\psi}{dq^2} + \left(\varepsilon - \kappa^2\frac{s^2}{c^2}\right)\psi = 0, \tag{9}$$

where $\varepsilon = \frac{2m_0E}{\alpha\hbar^2}$, $\kappa = \frac{m_0\omega}{\alpha\hbar}$, $c = \cos q$, $s = \sin q$.

Assuming $\psi(q) = c^\lambda f(s)$, the function $f(s)$ satisfies:

$$(1-s^2)\frac{d^2f}{ds^2} - (2\lambda+1)s\frac{df}{ds} + \left[(\varepsilon-\lambda) - \left(\kappa^2 - \lambda(\lambda-1)\right)\frac{s^2}{c^2}\right]f = 0. \tag{10}$$

To remove the singularity at $c = 0$, we impose:

$$\kappa^2 - \lambda(\lambda-1) = 0 \quad \Rightarrow \quad \lambda = \frac{1}{2} + \frac{1}{2}\sqrt{1+4\kappa^2}. \tag{11}$$

This reduces Eq. (10) to:

$$(1-s^2)\frac{d^2f}{ds^2} - (2\lambda+1)s\frac{df}{ds} + (\varepsilon-\lambda)f = 0. \tag{12}$$

Requiring polynomial solutions (to avoid singularities at $s = \pm1$) leads to the quantization condition:

$$\varepsilon - \lambda = n(n+2\lambda), \quad n \in \mathbb{N}. \tag{13}$$

Substituting back, the final expression for the energy spectrum becomes [36]:

$$E_n = \hbar\omega\left(n+\frac{1}{2}\right)\sqrt{1+\frac{\alpha^2\hbar^2}{4m_0^2\omega^2}} + \frac{\alpha\hbar^2}{2m_0}\left(n^2+2n+\frac{1}{2}\right). \tag{14}$$

3 Thermodynamics and Superstatistics Properties

In the thermodynamic and superstatistical analysis of a harmonic oscillator with position-dependent mass, calculating the partition function is a crucial step. It serves as a distribution function in statistical mechanics and provides access to the fundamental properties of the system.

3.1 Thermodynamics properties

This behavior suggests that α acts as a deformation or coupling parameter that enhances the confining potential or interaction strength, resulting in steeper energy scaling with the quantum number n.

The curves exhibit a convex profile, suggesting that the rate of increase in energy becomes more pronounced as α increases. This trend may reflect a growing confinement, curvature, or interaction strength in the system governed by α.

To evaluate the thermodynamic properties of a harmonic oscillator with position-dependent mass, the energy expression previously derived in Eq. (14) is rewritten in the compact form

$$E_n = a\left(n+\frac{1}{2}\right)+b\left(n^2+2n+\frac{1}{2}\right), \tag{15}$$

where

$$a=\hbar\omega\sqrt{1+\frac{\alpha^2\hbar^2}{4m_0^2\omega^2}}, \qquad b=\frac{\alpha\hbar^2}{2m_0\omega}. \tag{16}$$

Figures 1(a)–1(b) display the energy spectrum of the PDM harmonic oscillator as a function of the quantum number n and of the deformation parameter α. These results clearly demonstrate that the spectrum depends strongly on both parameters. For the three representative values $\alpha = 0.1, 0.3, 0.9$, the energy increases nonlinearly with n, and the rate of growth becomes significantly steeper as α increases. This means that the system becomes more energetically demanding for higher deformation, which reflects a stronger effective confinement.

Figure 1(b) shows that the energy levels increase monotonically with the deformation parameter α for each fixed value of n. Higher excited states ($n = 3, 5$) remain consistently above lower ones, confirming that energy grows with both α and the quantum number n. The convex shape of the curves indicates that the sensitivity of the spectrum to α becomes more pronounced for larger values of the deformation parameter, suggesting stronger curvature or interaction effects induced by the mass variation.

From a thermodynamic perspective, this behavior has important implications. Since all thermodynamic quantities are derived from the partition function

$$Z=\sum_{n=0}^{\infty} e^{-\beta E_n},$$

the nonlinear growth of the energy spectrum directly modifies the density of accessible states. Larger values of α increase the energy gap between successive levels, thereby reducing the number of states significantly populated at a given temperature. As a result, the entropy and specific heat are expected to decrease with increasing α, reflecting a more constrained and less thermally active system. Similarly, the free energy becomes more negative as the spectrum shifts upward, while the internal energy grows more slowly with temperature due to the reduced availability of low-energy states.

Overall, the deformation parameter α plays a central thermodynamic role: by controlling the curvature of the effective mass profile, it enhances the confinement of the system and modifies the thermal population of the states, leading to distinctive thermodynamic signatures.

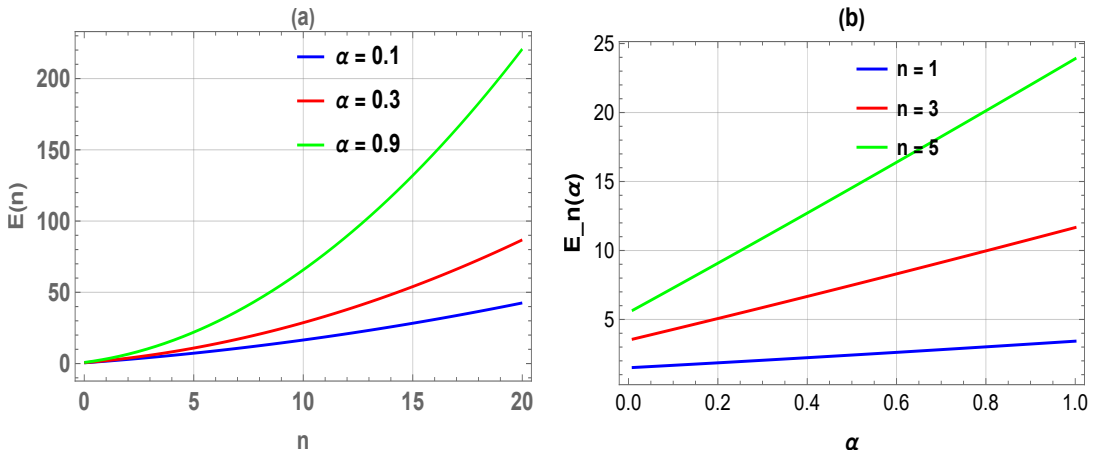

Figure 1: (a) Energy spectrum of the PDM harmonic oscillator as a function of the quantum number n for fixed values of the parameter α; (b) Energy spectrum as a function of the deformation parameter α for fixed values of the quantum number n.

Once the energy spectrum is expressed in a simplified form, one can readily proceed to the evaluation of the partition function, which serves as a basis for deriving the associated thermodynamic properties. For systems with bound states, the partition function is generally defined as follows equation [2,42–46].

$$Z(\beta) = \sum_{n=0}^{\infty} e^{-\beta E_n}, \quad \beta = \frac{1}{k_B T} \tag{17}$$

Where k_B is the Boltzmann constant and E_n is energy of the bound state. By inserting the expressions of the energy spectrum derived in Eq. (15) into Eq. (17), and using Mathematica 13.3 software, we obtain the α-deformed partition function within the framework of superstatistics for the position-dependent mass harmonic oscillator, in the presence of the deformation parameter α.

$$Z(\beta) = \frac{e^{\frac{(a^2+2ab+2b^2)}{4b}\beta}\sqrt{\pi}}{2\sqrt{b\beta}} \left(-\operatorname{Erf}\left[\frac{1}{2}(a+2b)\sqrt{\frac{\beta}{b}}\right] + \operatorname{Erf}\left[\frac{1}{2}(a+4b)\sqrt{\frac{\beta}{b}}\right]\right) \tag{18}$$

After a careful computation of the partition function associated with the model eq. (18), we now proceed to extract the corresponding thermodynamic quantities. Using the compact expression of the partition function $Z(\beta)$, the mean internal energy $U(\beta)$, the heat specific $C(\beta)$, the entropy $S(\beta)$ and the thermodynamic potentials such as the Helmholtz free energy $F(\beta)$, can be obtained from the standard thermodynamic identities [2,42–46]:

$$U(\beta) = -\frac{\partial(\ln Z(\beta))}{\partial\beta} \tag{19}$$

$$= \frac{e^{-3\beta-\frac{a^2\beta}{2b}-5b\beta}\left(2\sqrt{b\beta}\,e^{\frac{(a^2+2b)^2\beta}{4b}}\left(2b(-2+e^{(a+3b)\beta})+a(-1+e^{(a+3b)\beta})\right)\right.}{4b\beta\sqrt{\pi}\left(-\operatorname{Erf}\left[\frac{1}{2}(a+2b)\sqrt{\frac{\beta}{b}}\right]+\operatorname{Erf}\left[\frac{1}{2}(a+4b)\sqrt{\frac{\beta}{b}}\right]\right)}$$

$$+ \frac{\left.(a^2\beta+2b^2\beta+2b(-1+a\beta))\,e^{3a\beta+\frac{a^2\beta}{2b}+5b\beta}\sqrt{\pi}\left(\operatorname{Erf}\left[\frac{1}{2}(a+2b)\sqrt{\frac{\beta}{b}}\right]-\operatorname{Erf}\left[\frac{1}{2}(a+4b)\sqrt{\frac{\beta}{b}}\right]\right)\right)}{4b\beta\sqrt{\pi}\left(-\operatorname{Erf}\left[\frac{1}{2}(a+2b)\sqrt{\frac{\beta}{b}}\right]+\operatorname{Erf}\left[\frac{1}{2}(a+4b)\sqrt{\frac{\beta}{b}}\right]\right)} \tag{20}$$

$$
\begin{aligned}
C(\beta) &= k_B\beta^2\frac{\partial^2}{\partial\beta^2}\ln Z(\beta) && (21)\\
&= \Bigg(\beta e^{-5a\beta-\frac{3a^2\beta}{4b}-9b\beta}\Bigg[2b\beta\sqrt{\frac{\beta}{b}}e^{\frac{(a+2b)^2\beta}{4b}}\left(a-ae^{(a+3b)\beta}-2b(-2+e^{(a+3b)\beta})\right)^2\\
&- 4b\sqrt{b\beta}e^{5a\beta+\frac{3a^2\beta}{4b}+9b\beta}\pi\,\mathrm{Erf}\left[\frac{1}{2}(a+2b)\sqrt{\frac{\beta}{b}}\right]^2-\beta e^{3a\beta+\frac{a^2\beta}{2b}+5b\beta}\\
&\times \Bigg(6a^2b\beta(-2+e^{(a+3b)\beta})+a^3\beta(-1+e^{(a+3b)\beta})+4b^2\Bigg(-2+e^{(a+3b)\beta}+2b\beta\Bigg(-8\\
&+ e^{(a+3b)\beta}\Bigg)\Bigg)+2ab(-1+e^{(a+3b)\beta}+6b\beta(-4+e^{(a+3b)\beta}))\Bigg)\sqrt{\pi}\,\mathrm{Erf}\left[\frac{1}{2}(a+4b)\sqrt{\frac{\beta}{b}}\right]\\
&- 4b\sqrt{b\beta}e^{5a\beta+\frac{3a^2\beta}{4b}+9b\beta}\pi\,\mathrm{Erf}\left[\frac{1}{2}(a+4b)\sqrt{\frac{\beta}{b}}\right]^2+\sqrt{\pi}\,\mathrm{Erf}\left[\frac{1}{2}(a+2b)\sqrt{\frac{\beta}{b}}\right]\\
&\times \beta e^{3a\beta+\frac{a^2\beta}{2b}+5b\beta}\Bigg(6a^2b\beta(-2+e^{(a+3b)\beta})+a^3\beta(-1+e^{(a+3b)\beta})+4b^2\Bigg(-2+e^{(a+3b)\beta}\\
&+ 2b\beta(-8+e^{(a+3b)\beta})\Bigg)+2ab(-1+e^{(a+3b)\beta})+6b\beta(-4+e^{(a+3b)\beta})\Bigg)\\
&+ 8b\sqrt{b\beta}e^{5a\beta+\frac{3a^2\beta}{4b}+9b\beta}\sqrt{\pi}\,\mathrm{Erf}\left[\frac{1}{2}(a+4b)\sqrt{\frac{\beta}{b}}\right]\Bigg)\\
&\Bigg/\left(8(b\beta)^{3/2}\pi\left(\mathrm{Erf}\left[\frac{1}{2}(a+2b)\sqrt{\frac{\beta}{b}}\right]-\mathrm{Erf}\left[]\frac{1}{2}(a+4b)\sqrt{\frac{\beta}{b}}\right]\right)^2\right) && (22)
\end{aligned}
$$

$$
\begin{aligned}
S(\beta) &= k_B\ln Z(\beta)-k_B\beta\frac{\partial(\ln Z(\beta))}{\partial\beta} && (23)\\
&= \Bigg(\sqrt{\frac{\beta}{b}}e^{-3a\beta-\frac{a^2\beta}{2b}-5b\beta}\Bigg(2\beta e^{\frac{(a+2b)^2\beta}{4b}}(a-ae^{(a+3b)\beta}-2b(-2+e^{(a+3b)\beta})\Bigg)\\
&- \sqrt{\frac{\beta}{b}}(a^2\beta+2b^2\beta+2b(-1+a\beta))e^{3a\beta+\frac{a^2\beta}{2b}+5b\beta}\sqrt{\pi}\,\mathrm{Erf}\left[\frac{1}{2}(a+2b)\sqrt{\frac{\beta}{b}}\right]\\
&+ \sqrt{\frac{\beta}{b}}\Bigg(a^2\beta+2b^2\beta+2b(-1+a\beta)\Bigg)e^{3a\beta+\frac{a^2\beta}{2b}+5b\beta}\sqrt{\pi}\,\mathrm{Erf}\left[\frac{1}{2}(a+4b)\sqrt{\frac{\beta}{b}}\right]\Bigg)\Bigg)\Bigg/\\
&\Bigg(4\beta\pi\Bigg(\mathrm{Erf}\left[\frac{1}{2}(a+2b)\sqrt{\frac{\beta}{b}}\right]-\mathrm{Erf}\left[\frac{1}{2}(a+4b)\sqrt{\frac{\beta}{b}}\right]\Bigg)\Bigg)\\
&+\log\left(\frac{e^{\frac{(a^2+2ab+2b^2)\beta}{4b}}\sqrt{\pi}\left(-\mathrm{Erf}\left[\frac{1}{2}(a+2b)\sqrt{\frac{\beta}{b}}\right]+\mathrm{Erf}\left[\frac{1}{2}(a+4b)\sqrt{\frac{\beta}{b}}\right]\right)}{2\sqrt{b\beta}}\right). && (24)
\end{aligned}
$$

$$
\begin{aligned}
F(\beta) &= -\frac{1}{\beta}\ln Z(\beta) && (25)\\
&= -\frac{1}{\beta}\log\left(\frac{e^{\frac{(a^2+2ab+2b^2)\beta}{4b}}\sqrt{\pi}\left(-\mathrm{Erf}\left[\frac{1}{2}(a+2b)\sqrt{\frac{\beta}{b}}\right]+\mathrm{Erf}\left[\frac{1}{2}(a+4b)\sqrt{\frac{\beta}{b}}\right]\right)}{2\sqrt{b\beta}}\right) && (26)
\end{aligned}
$$

3.2 Superstatistics Properties

Superstatistics is a statistical framework developed to describe driven, non-equilibrium systems characterized by fluctuations in intensive parameters, such as the inverse temperature β, chemical potential, or energy [47–50]. These fluctuations occur over spatiotemporal scales and are typically captured by extending the conventional Boltzmann factor into a more general form known as the *effective Boltzmann factor* [50–53].

In this context, superstatistics can be viewed as a superposition of different local equilibrium statistics. The standard approach involves taking the Laplace transform of the probability density function $f(\beta')$, which results in the generalized Boltzmann factor [51, 53]:

$$B_E(\beta) = \int_0^\infty e^{-\beta' E} f(\beta', \beta)\, d\beta'. \tag{27}$$

When $f(\beta', \beta)$ is modeled by a Dirac delta function $\delta(\beta - \beta')$, the integral simplifies, and a deformation parameter q can be introduced to yield the generalized Boltzmann factor:

$$B_E^{(q)}(\beta) = e^{-\beta E}\left(1 + \frac{q}{2}\beta^2 E^2\right). \tag{28}$$

Here, $q \in [0, 1]$ is a deformation parameter that quantifies the departure from classical Boltzmann-Gibbs statistics. In the limit $q \to 0$, standard statistical mechanics is recovered.

The partition function in the superstatistical framework is then defined as:

$$Z_s = \int_0^\infty B_E^{(q)}(\beta)\, dn. \tag{29}$$

For discrete systems, such as quantum harmonic oscillators, this can be written as a summation over energy levels:

$$Z = \sum_{n=0}^{\infty} B_E(n\beta). \tag{30}$$

At high temperature limits ($T \gg 1$), the discrete summation may be approximated by an integral to simplify analysis.

When applied to specific systems like the harmonic oscillator with position-dependent mass, this formalism enables the derivation of modified thermodynamic quantities. These generalized functions are valid for all values of q and explicitly depend on the system's energy spectrum. Thus, superstatistics provides a robust framework for analyzing complex, non-linear, and far-from-equilibrium systems where traditional statistical mechanics falls short.

Using Eq.(29)and Mathematica 13.3, the superstatistics partition function equation is given as

$$\begin{aligned}
Z_s(a,b,\beta,q) &= \frac{1}{64b^{5/2}\sqrt{\beta}} e^{-\frac{1}{2}(a+b)\beta}\Bigg(\sqrt{\beta}\Bigg(12ab^{3/2} + 24b^{5/2} - 2a^3\sqrt{b}\beta + a^4\beta^{3/2} \\
&\times\ e^{\frac{(a+2b)^2\beta}{4b}}\sqrt{\pi}\Bigg)q - 4a^2b\beta\Bigg(\sqrt{b\beta} + (1-a\beta)e^{\frac{(a+2b)^2\beta}{4b}}\sqrt{\pi}\Bigg)q + 4b^4\beta^2 e^{\frac{(a+2b)^2\beta}{4b}}\sqrt{\pi}q \\
&+\ 8b^3\beta(-1+a\beta)e^{\frac{(a+2b)^2\beta}{4b}}\sqrt{\pi}q + 4b^2 e^{\frac{(a+2b)^2\beta}{4b}}\sqrt{\pi}\Bigg(8 + (3 - 2a\beta + 2a^2\beta^2)q\Bigg) \\
&-\ e^{\frac{(a+2b)^2\beta}{4b}}\sqrt{\pi}\Bigg(a^4\beta^2 q + 4b^4\beta^2 q + 4a^2b\beta(-1+a\beta)q + 8b^3\beta(-1+a\beta)q \\
&+\ 4b^2\Bigg(8 + (3 - 2a\beta + 2a^2\beta^2)q\Bigg)\mathrm{Erf}\left[\frac{(a+2b)\beta}{2\sqrt{b\beta}}\right]\Bigg)\Bigg).
\end{aligned} \tag{31}$$

Using the Superstatistic partition function in Eq.(31), the Superstatistics thermodynamics properties are obtained as follows.

1. Vibrational mean energy

$$
\begin{aligned}
U_s(a,b,\beta,q) &= -\frac{\partial}{\partial\beta}\ln Z_s(\beta) \qquad (32)\\
&= -\Big[4a^3\Big(-2b^{3/2}\beta^{3/2}\sqrt{b\beta}+b^{5/2}\beta^{5/2}\sqrt{b\beta}+2b^2\beta^2\left(1+\sqrt{b\beta}e^{\frac{(a+2b)^2\beta}{4b}}\sqrt{\pi}\right)\\
&\quad +2b^3\beta^3\left(-3+4\sqrt{b\beta}e^{\frac{(a+2b)^2\beta}{4b}}\sqrt{\pi}\right)\Big)q\\
&\quad +2a^5b\beta^3\left(-1+3\sqrt{b\beta}e^{\frac{(a+2b)^2\beta}{4b}}\sqrt{\pi}\right)q+2a^4b\beta^2\Big(-4b\beta+\sqrt{b\beta}e^{\frac{(a+2b)^2\beta}{4b}}\sqrt{\pi}\\
&\quad +9b^{3/2}\beta^{3/2}e^{\frac{(a+2b)^2\beta}{4b}}\sqrt{\pi}\Big)q+a^6\beta^3\sqrt{b\beta}e^{\frac{(a+2b)^2\beta}{4b}}\sqrt{\pi}q+8ab^2\beta\Big(-8\\
&\quad -\left(3+3b\beta+5b^2\beta^2\right)q+\sqrt{b\beta}e^{\frac{(a+2b)^2\beta}{4b}}\sqrt{\pi}\left(8+q+2b\beta q+3b^2\beta^2q\right)\Big)\\
&\quad +4a^2b^2\beta\Big(-2b\beta q-10b^2\beta^2q+\sqrt{b\beta}e^{\frac{(a+2b)^2\beta}{4b}}\sqrt{\pi}(8+q+4b\beta q+9b^2\beta^2q)\Big)\\
&\quad +8b^3\Big(-6b^{3/2}\beta^{3/2}\sqrt{b\beta}q+b^3\beta^3\Big(-2+\sqrt{b\beta}e^{\frac{(a+2b)^2\beta}{4b}}\sqrt{\pi}\Big)q\\
&\quad +b^2\beta^2\left(4+\sqrt{b\beta}e^{\frac{(a+2b)^2\beta}{4b}}\sqrt{\pi}\right)q-\sqrt{b\beta}e^{\frac{(a+2b)^2\beta}{4b}}\sqrt{\pi}(8+3q)\\
&\quad +b\beta\left(\sqrt{b\beta}e^{\frac{(a+2b)^2\beta}{4b}}\sqrt{\pi}(8+q)-2(8+3q)\right)\Big)-\sqrt{b\beta}\Big(a^2\beta+2b^2\beta\\
&\quad +2b(-1+a\beta)\Big)e^{\frac{(a+2b)^2\beta}{4b}}\sqrt{\pi}\Big(a^4\beta^2q+4b^4\beta^2q+4a^2b\beta(1+a\beta)q\\
&\quad +8b^3\beta(1+a\beta)q+4b^2\Big(8+(3+2a\beta+2a^2\beta^2)q\Big)\Big)\mathrm{Erf}\left[\frac{(a+2b)\beta}{2\sqrt{b\beta}}\right]\Big]\Big/\\
&\Big[4b^{3/2}\beta^{3/2}\Big(12ab^{3/2}\sqrt{\beta}q+24b^{5/2}\sqrt{\beta}q-2a^3\sqrt{b}\beta^{3/2}q-4a^2b\beta\Big(\sqrt{b\beta}\\
&\quad +(1-a\beta)e^{\frac{(a+2b)^2\beta}{4b}}\sqrt{\pi}\Big)q+a^4\beta^2e^{\frac{(a+2b)^2\beta}{4b}}\sqrt{\pi}q+4b^4\beta^2e^{\frac{(a+2b)^2\beta}{4b}}\sqrt{\pi}q\\
&\quad +8b^2\beta(-1+a\beta)e^{\frac{(a+2b)^2\beta}{4b}}\sqrt{\pi}q+4b^2e^{\frac{(a+2b)^2\beta}{4b}}\sqrt{\pi}\Big(8\\
&\quad +(3-2a\beta+2a^2\beta^2)q\Big)-e^{\frac{(a+2b)^2\beta}{4b}}\sqrt{\pi}\Big(a^4\beta^2q+4b^4\beta^2q\\
&\quad +4a^2b\beta(-1+a\beta)q+8b^3\beta(-1+a\beta)q\\
&\quad +4b^2\Big(8+(3-2a\beta+2a^2\beta^2)q\Big)\Big)\mathrm{Erf}\left[\frac{(a+2b)\beta}{2\sqrt{b\beta}}\right]\Big)\Big]. \qquad (33)
\end{aligned}
$$

2. Free energy

$$
\begin{aligned}
F_s(a,b,\beta,q) &= -\frac{1}{\beta}\ln Z_s(\beta) \\
&= -\frac{1}{\beta}\times\ln\Bigg(\frac{1}{64b^{5/2}\sqrt{\beta}}e^{-\frac{1}{2}(a+b)\beta}\Bigg(\sqrt{\beta}\Bigg(12ab^{3/2}+24b^{5/2}+2a^3\sqrt{b}\beta+a^4\beta^{3/2} \\
&\times\ e^{\frac{(a+2b)^2\beta}{4b}}\sqrt{\pi}\Bigg)q-4a^2b\beta\Bigg(\sqrt{b\beta}+(1-a\beta)e^{\frac{(a+2b)^2\beta}{4b}}\sqrt{\pi}\Bigg)q+4b^4\beta^2e^{\frac{(a+2b)^2\beta}{4b}}\sqrt{\pi}q \\
&+\ 8b^3\beta(-1+a\beta)e^{\frac{(a+2b)^2\beta}{4b}}\sqrt{\pi}q+4b^2e^{\frac{(a+2b)^2\beta}{4b}}\sqrt{\pi}\Bigg(8+(3-2a\beta+2a^2\beta^2)q\Bigg) \\
&-\ e^{\frac{(a+2b)^2\beta}{4b}}\sqrt{\pi}\Bigg(a^4\beta^2q+4b^4\beta^2q+4a^2b\beta(-1+a\beta)q+8b^3\beta(-1+a\beta)q \qquad (34)\\
&+\ 4b^2\Bigg(8+(3-2a\beta+2a^2\beta^2)q\Bigg)\mathrm{Erf}\Bigg[\frac{(a+2b)\beta}{2\sqrt{b\beta}}\Bigg]\Bigg)\Bigg)\Bigg).
\end{aligned}
$$

3. Entropy

$$
\begin{aligned}
S_s(a,b,\beta,q) &= k_B\Bigg(-\beta\Bigg(4a^3\Bigg(-2b^{3/2}\beta^{3/2}\sqrt{b\beta}+b^{5/2}\beta^{5/2}\sqrt{b\beta}+2b^2\beta^2\Bigg(1 \\
&+\ \sqrt{b\beta}e^{\frac{(a+2b)^2\beta}{4b}}\sqrt{\pi}\Bigg)+2b^3\beta^3\left(-3+4\sqrt{b\beta}e^{\frac{(a+2b)^2\beta}{4b}}\sqrt{\pi}\right)\Bigg)q \\
&+\ 2a^5b\beta^3\left(-1+3\sqrt{b\beta}e^{\frac{(a+2b)^2\beta}{4b}}\sqrt{\pi}\right)q \\
&+\ 2a^4b\beta^2\left(-6b\beta+b\beta+\sqrt{b\beta}e^{\frac{(a+2b)^2\beta}{4b}}\sqrt{\pi}+9(b\beta)^{3/2}e^{\frac{(a+2b)^2\beta}{4b}}\sqrt{\pi}\right)q \\
&+\ a^6\beta^3\sqrt{b\beta}e^{\frac{(a+2b)^2\beta}{4b}}\sqrt{\pi}q+8ab^3\beta\Bigg(-8-(3+3b\beta+5b^2\beta^2)q \\
&+\ \sqrt{b\beta}e^{\frac{(a+2b)^2\beta}{4b}}\sqrt{\pi}(8+q+2b\beta q+3b^2\beta^2q)\Bigg) \\
&+\ 4a^2b^2\beta\Bigg(-2b\beta q-10b^2\beta^2q \\
&+\ \sqrt{b\beta}e^{\frac{(a+2b)^2\beta}{4b}}\sqrt{\pi}(8+q+4b\beta q+9b^2\beta^2q)\Bigg) \\
&+\ 8b^3\Bigg(-6b^{3/2}\beta^{3/2}\sqrt{b\beta}q+b^3\beta^3\left(-2+\sqrt{b\beta}e^{\frac{(a+2b)^2\beta}{4b}}\sqrt{\pi}\right)q \\
&+\ b^2\beta^2\left(4+\sqrt{b\beta}e^{\frac{(a+2b)^2\beta}{4b}}\sqrt{\pi}\right)q-\sqrt{b\beta}e^{\frac{(a+2b)^2\beta}{4b}}\sqrt{\pi}(8+3q)
\end{aligned}
$$

$$
\begin{aligned}
&+ \quad b\beta\left(\sqrt{b\beta}e^{\frac{(a+2b)^2\beta}{4b}}\sqrt{\pi}(8+q)-2(8+3q)\right)\Bigg) \\
&- \quad \sqrt{b\beta}(a^2\beta+2b^2\beta+2b(-1+a\beta))e^{\frac{(a+2b)^2\beta}{4b}}\sqrt{\pi} \\
&\quad \times\Bigg(a^4\beta^2q+4b^4\beta^2q+4a^2b\beta(1+a\beta)q+8b^3\beta(1+a\beta)q+4b^2(8 \\
&+ \quad (3+2a\beta+2a^2\beta^2)q)\Bigg)\mathrm{Erf}\left(\frac{(a+2b)\beta}{2\sqrt{b\beta}}\right)\Bigg)\Bigg/\Bigg(4(b\beta)^{3/2}\Bigg(\\
&\quad 12ab^{3/2}\sqrt{\beta}q+24b^{5/2}\sqrt{\beta}q-2a^3\sqrt{b}\beta^{3/2}q \\
&- \quad 4a^2b\beta\left(\sqrt{b\beta}+(1-a\beta)e^{\frac{(a+2b)^2\beta}{4b}}\sqrt{\pi}\right)q \\
&+ \quad a^4\beta^2e^{\frac{(a+2b)^2\beta}{4b}}\sqrt{\pi}q+4b^4\beta^2e^{\frac{(a+2b)^2\beta}{4b}}\sqrt{\pi}q \\
&+ \quad 8b^3\beta(-1+a\beta)e^{\frac{(a+2b)^2\beta}{4b}}\sqrt{\pi}q \\
&+ \quad 4b^2e^{\frac{(a+2b)^2\beta}{4b}}\sqrt{\pi}(8+(3-2a\beta+2a^2\beta^2)q) \\
&- \quad e^{\frac{(a+2b)^2\beta}{4b}}\sqrt{\pi}\Bigg(a^4\beta^2q+4b^4\beta^2q+4a^2b\beta(-1+a\beta)q \\
&+ \quad 8b^3\beta(-1+a\beta)q+4b^2(8+(3-2a\beta+2a^2\beta^2)q)\Bigg) \\
&\quad \times\mathrm{Erf}\left[\frac{(a+2b)\beta}{2\sqrt{b\beta}}\right]\Bigg)\Bigg)+\ln\left[\frac{1}{64b^{5/2}\sqrt{\beta}}e^{-\frac{1}{2}(a+b)\beta}\right. \\
&\times \quad \Bigg(\sqrt{\beta}\left(12ab^{3/2}+24b^{5/2}-2a^3\sqrt{b}\beta+a^4\beta^{3/2}e^{\frac{(a+2b)^2\beta}{4b}}\sqrt{\pi}\right)q \\
&- \quad 4a^2b\beta\left(\sqrt{b\beta}+(1-a\beta)e^{\frac{(a+2b)^2\beta}{4b}}\sqrt{\pi}\right)q \\
&+ \quad 4b^4\beta^2e^{\frac{(a+2b)^2\beta}{4b}}\sqrt{\pi}q+8b^3\beta(-1+a\beta)e^{\frac{(a+2b)^2\beta}{4b}}\sqrt{\pi}q \\
&+ \quad 4b^2e^{\frac{(a+2b)^2\beta}{4b}}\sqrt{\pi}(8+(3-2a\beta+2a^2\beta^2)q) \\
&- \quad e^{\frac{(a+2b)^2\beta}{4b}}\sqrt{\pi}\Bigg(a^4\beta^2q+4b^4\beta^2q+4a^2b\beta(-1+a\beta)q \\
&+ \quad 8b^3\beta(-1+a\beta)q+4b^2(8+(3-2a\beta+2a^2\beta^2)q)\Bigg)\mathrm{Erf}\left[\frac{(a+2b)\beta}{2\sqrt{b\beta}}\right]\Bigg)\Bigg] \qquad (35)
\end{aligned}
$$

4. Specific heat capacity

$$C_s(a,b,\beta,q)=k_B\beta^2\frac{\partial^2}{\partial\beta^2}\ln Z_s(a,b,\beta,q) \qquad (36)$$

4 Numerical results and discussion

Statistical properties

The figures Fig.2(a) and Fig.2(b) investigates the behavior of the partition function Z, a central quantity in statistical mechanics that encapsulates the thermodynamic properties of the system. In Fig.2(a), $Z(\beta)$ is plotted as a function of inverse temperature β for three distinct values of the interaction parameter α (0.1, 0.3, and 0.9). The partition function exhibits a monotonically decreasing trend with increasing β, reflecting the reduction in accessible microstates as the system approaches lower temperatures. Additionally, higher values of α lead to significantly lower values of Z, suggesting that the interaction term governed by α suppresses the system's configurational entropy and reduces the

number of energetically favorable states. In Fig.2(b), the focus shifts to the behavior of Z as a function of α, for fixed values of $\beta = 2, 5$, and 8. Here, $Z(\alpha)$ is a decreasing function, with steeper declines observed for larger β, i.e., lower temperatures. This reinforces the interpretation that the parameter α acts to constrain the phase space, particularly at lower thermal energies. The observed smoothness and regularity of the partition function across both figures suggest a well-defined thermodynamic regime without singularities, consistent with non-critical systems. Overall, these plots underscore the fundamental role of α in shaping the statistical weight of accessible states and demonstrate the interplay between thermal excitation and interaction strength in governing the equilibrium behavior of the system.

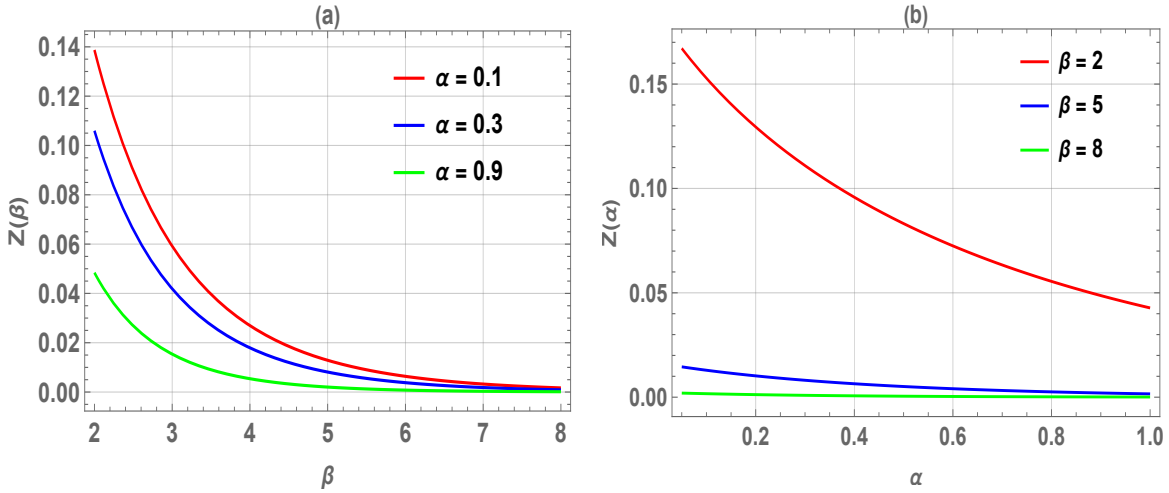

Figure 2: (The left panel(a), the partition function Z is displayed as a function of Inverse temperature parameter β, for various and fixed values of α, and . (The right panel(b), the partition function Z is displayed as a function of α, for various values of parameter β which take tree valuers $2, 5$ and 8

.

The Fig.3 provide insight into the thermal evolution of the average energy U, a key thermodynamic observable, as a function of inverse temperature β and interaction parameter α. In Fig.3(a), $U(\beta)$ is shown for three values of α: 0.1, 0.3, and 0.9. The energy decreases monotonically with increasing β, which corresponds to decreasing temperature, indicating that the system tends toward lower energy states as thermal agitation diminishes. For all values of β, higher values of α consistently produce lower energies, reflecting the stabilizing influence of this parameter and suggesting that it enhances the tendency of the system to occupy energetically favorable configurations. In contrast, Fig.3(b) examines $U(\alpha)$ for fixed values of β (2, 5, and 10). Here, the average energy increases with α, which might at first seem contradictory; however, this likely arises from a different scaling or parameter dependence in this specific model. At higher β (lower temperatures), the energy remains lower overall but still shows a rising trend with increasing α. This implies that although α generally acts as a stabilizing factor when the temperature varies, it also influences the energy landscape in a non-trivial way when held against a fixed thermal background. These results highlight the multifaceted role of α in the thermodynamic behavior of the system, which governs both the depth and the accessibility of the energy minima. The smooth and monotonic nature of both plots further reinforces the picture of a well-behaved equilibrium system with no apparent phase transitions within the explored parameter range.

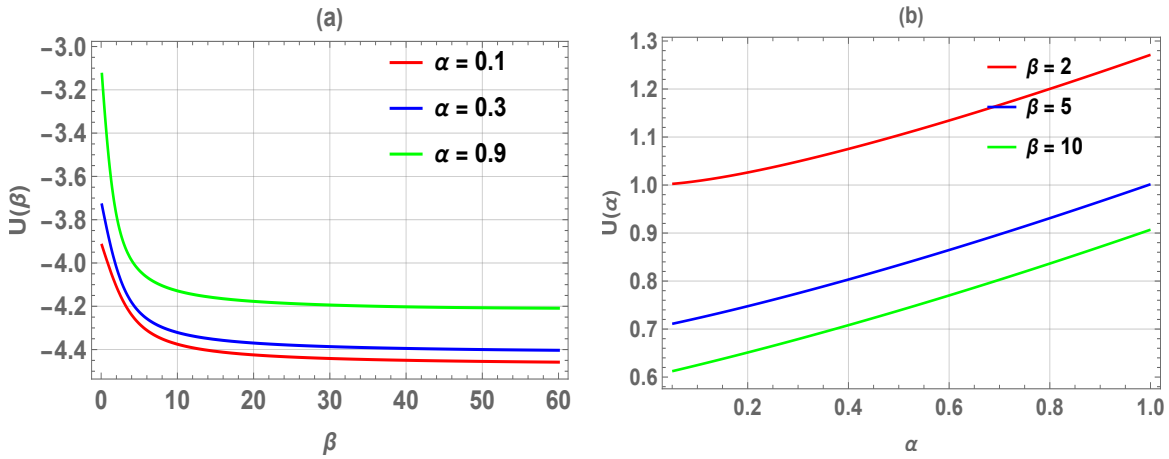

Figure 3: : (The left panel(a), the mean energy U is displayed as a function of for various values of Inverse temperature parameter β, and . (The right panel(b), the mean energy is displayed as a function of α, for various values of deformed parameter β.

The Fig4 provide complementary views of the system's heat capacity C, highlighting its dependence on the inverse temperature β and the interaction parameter α. In Fig.4(a), $C(\beta)$ is plotted for three values of α: 0.1, 0.3, and 0.9. The heat capacity increases sharply at first with β, suggesting a rapid enhancement of thermal sensitivity at lower temperatures, before reaching a saturation regime where additional increases in β yield diminishing returns in C. This behavior is indicative of a system transitioning from a disordered high-temperature regime to a more rigid low-temperature phase where thermal excitations become increasingly suppressed. As expected, larger values of α result in reduced heat capacity, implying that stronger interactions (or coupling) constrain the degrees of freedom available for thermal energy storage. In Fig.4(b), the heat capacity is examined as a function of α, for three fixed values of β: 0.5, 1, and 2. In this representation, $C(\alpha)$ decreases monotonically with increasing α, again confirming that greater coupling leads to a stiffer, less thermally responsive system. Furthermore, the influence of β is evident: lower values of β (i.e., higher temperatures) correspond to higher capacities, as thermal fluctuations dominate. Together, the two figures portray a consistent thermodynamic narrative where the heat capacity reflects the interplay between thermal agitation and interaction-induced rigidity. The smooth and monotonic trends in both plots suggest a lack of critical phenomena and instead support a continuously varying, well-behaved response typical of analytically tractable models.

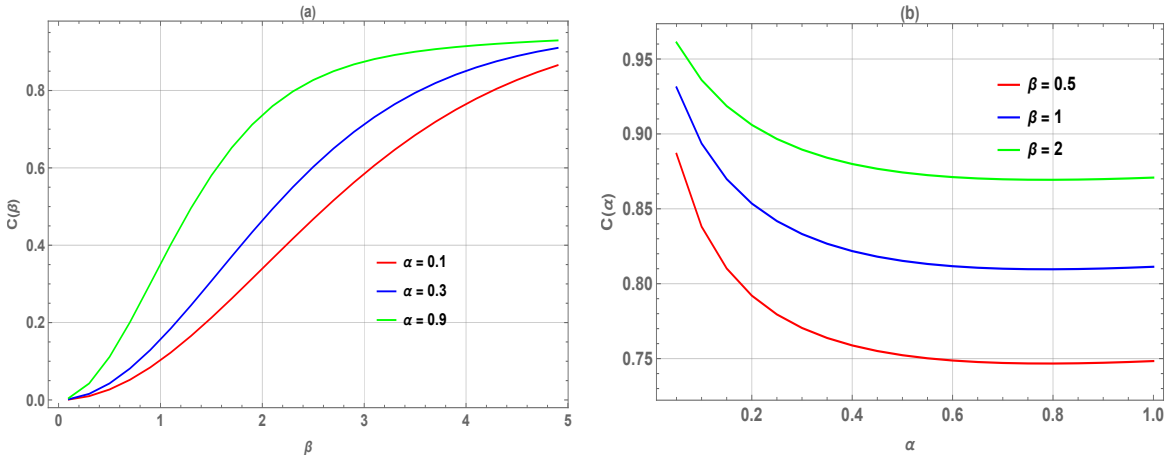

Figure 4: (The left panel(a), the specific heat C is displayed as a function of for various values of Inverse temperature parameter β, and (The right panel(b), is displayed as a function of C, for various values of α for fixed deformed parameter β.

The two Fig.5 depict the thermodynamic behavior of entropy S as a function of inverse temperature

β and the interaction parameter α, respectively. In Fig.5(a), $S(\beta)$ is shown for three values of α: 0.1, 0.3, and 0.9. The entropy decreases monotonically as β increases, consistent with the fundamental thermodynamic principle that entropy diminishes at lower temperatures due to a reduction in accessible microstates. Furthermore, for any fixed β, increasing α results in lower entropy values, indicating that the interaction parameter α effectively constrains the configurational degrees of freedom of the system. The entropy values are notably small and negative, on the order of 10^{-24}, which suggests the use of a relative entropy scale or a renormalized reference state. Fig.5(b), on the other hand, presents $S(\alpha)$ for fixed values of $\beta = 0.2, 0.5$, and 1.0. In this case, entropy increases significantly with α, particularly at lower β (i.e., higher temperatures), reflecting a regime where interaction strength enhances rather than suppresses entropy. This seemingly contrasting trend can be interpreted as a reflection of the dual influence of α and β: at high thermal energies, increasing α may broaden the distribution of accessible states, thus increasing entropy. Overall, the results suggest that the entropy's dependence on α is temperature-sensitive and non-monotonic across thermal regimes. The smooth evolution and absence of singular behavior in both figures affirm the analytic nature of the underlying model and its suitability for controlled thermodynamic analysis.

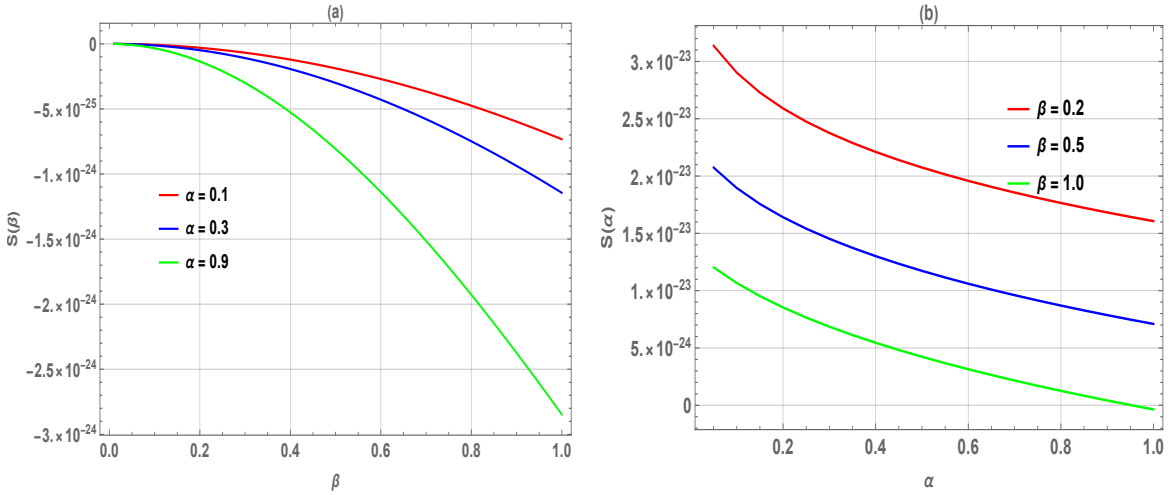

Figure 5: : (The left pane(a)), the entropy S is displayed as a function of Inverse temperature parameter β for various values of α, and (The right panel(b), is displayed as a function of α, for various values of deformed parameter β.

The two Fig.6 offer a thermodynamic analysis of the Helmholtz free energy F, plotted respectively as a function of inverse temperature β and the interaction parameter α. In Fig.6(a), $F(\beta)$ is illustrated for three values of α: 0.1, 0.3, and 0.9. The free energy increases monotonically with β, which corresponds to decreasing temperature, reflecting the growing contribution of internal energy as thermal disorder subsides. For any fixed β, larger values of α yield lower values of F, indicating a stabilizing influence of this interaction parameter that reduces the system's overall thermodynamic potential. The behavior is smooth and nearly linear, suggesting an absence of abrupt transitions. In Fig.6(b), $F(\alpha)$ is shown for fixed values of $\beta = 0.2, 0.5$, and 1.0. In contrast to Fig.6(a), the free energy here decreases as α increases, with curves exhibiting a quasi-linear descent whose steepness depends on the value of β. For lower β (higher temperatures), the free energy remains positive, while at higher β, F becomes negative for larger α, signifying a stronger stabilizing effect at lower temperatures. This dual representation reveals how the interplay between thermal energy and interaction strength governs the system's equilibrium configuration. The consistent monotonicity and smooth gradients in both graphs affirm the analytic and stable character of the model, indicative of a system that remains far from critical points within the explored parameter space.

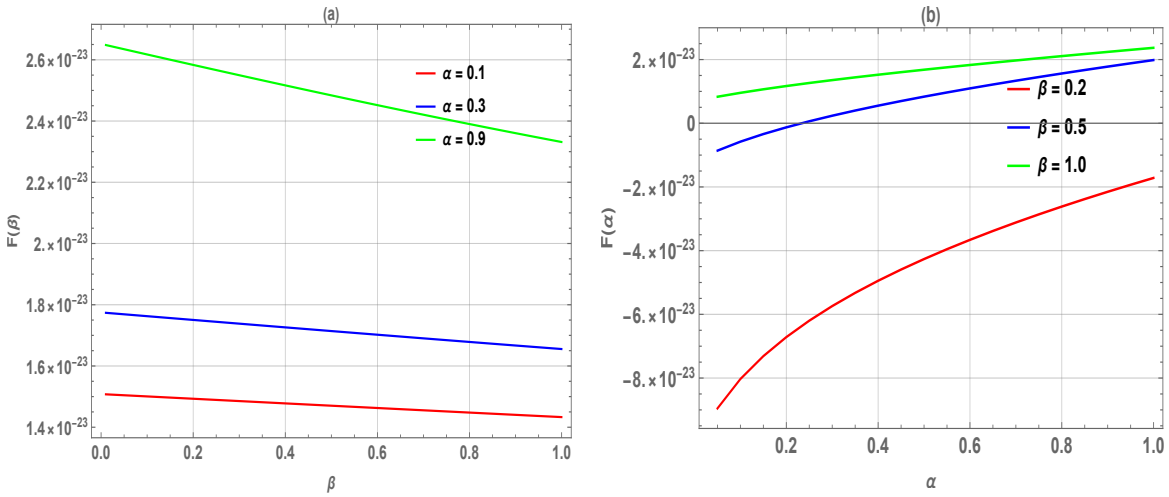

Figure 6: : (The left panel(a), the free energy F is displayed for various values of α as a function of Inverse temperature parameter β, and (The right panel(b), is displayed as a function of α, for various values of deformed parameter β.

Superstatistic properties

Figures Fig.7(a) and (b) illustrate the behavior of the supertatistic partition function Z_s as a function of the inverse temperature β an the deformation parameter α respectively. In Fig.7(b), Z_s decreases monotonically with increasing α, indicating that mass deformation reduces the number of accessible microstates by introducing geometric constraints. This suppression becomes more pronounced at higher β (i.e., lower temperatures). Fig.7(a) shows that Z_s increases with β, consistent with the thermal occupation of low-energy states, but this growth is significantly dampened for larger α. Overall, the results highlight that α acts as a superstatistical parameter that modulates thermal accessibility and energy-level sensitivity of the system.

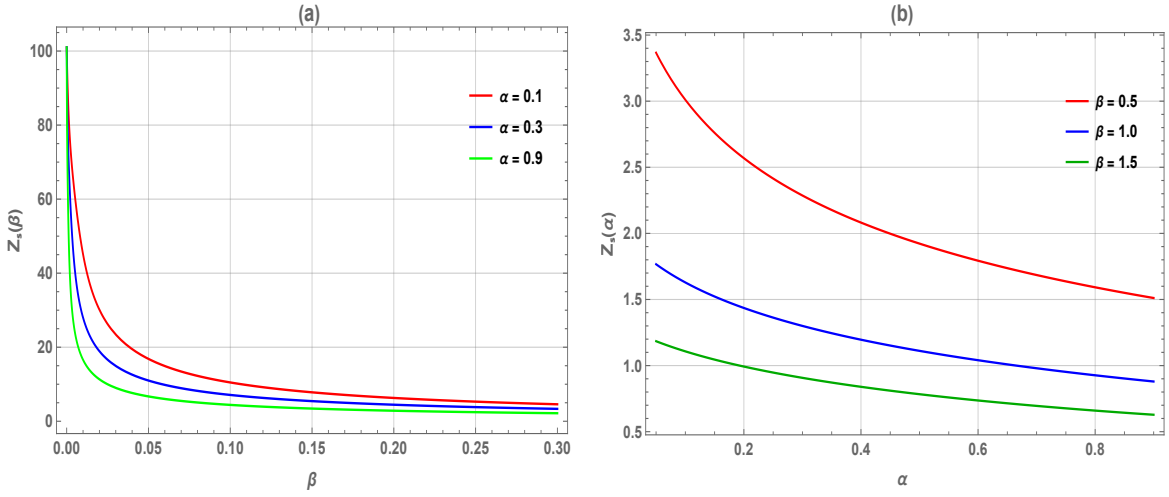

Figure 7: (The left panel(a), the superstatistical partition function Z_s is displayed as a function of Inverse temperature parameter β, for various and fixed values of α, and . (The right panel(b), this partition function Z_s is displayed as a function of α, for various values of parameter β which take tree valuers $0.5, 1.0$ and 1.5

Fig.8(a) and (b) present the behavior of the superstatistical internal energy U_s as a function of the inverse temperature β and the deformation parameter α, respectively. In Fig.8(a), $U_s(\beta)$ decreases monotonically as β increases, consistent with the thermal depopulation of higher energy states at

lower temperatures. The magnitude of this decrease is more pronounced for lower α, showing that less deformed systems are more thermally responsive. In Fig.8(b), $U_s(\alpha)$ increases rapidly with α, especially at higher β, indicating that mass deformation leads to a steeper energy spectrum and higher excitation energy. This reveals that α enhances confinement and raises the overall energy cost to populate quantum states. These trends confirm the role of α as a structural control parameter influencing the thermodynamic rigidity of the system.

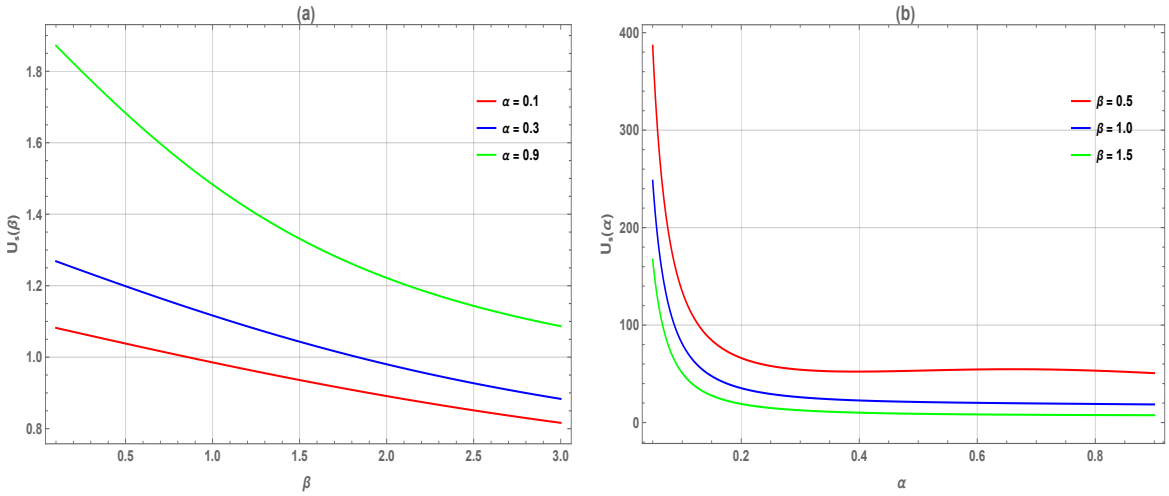

Figure 8: : (The left panel(a), the superstatistic mean energy U_s is displayed as a function of for various values of Inverse temperature parameter β, and . (The right panel(b) in a function of α, for various values of deformed parameter β.

The Fig.9(a) and (b) illustrate the dependence of the superstatistic entropy S_s on the inverse temperature β and the deformation parameter α, respectively. In Figure (a), S_s increases with β, reflecting the enhanced thermal population of energy levels and greater statistical disorder at lower temperatures. However, systems with higher α exhibit consistently lower entropy, suggesting that deformation suppresses the number of accessible microstates. Figure (b) shows that S_s decreases steadily as α increases, with this decline becoming sharper at higher values of β. This behavior indicates that mass deformation acts as an ordering mechanism, restricting phase space and limiting thermodynamic fluctuations. Overall, the results emphasize the role of α as a controlling parameter that reduces entropy, especially in low-temperature regimes.

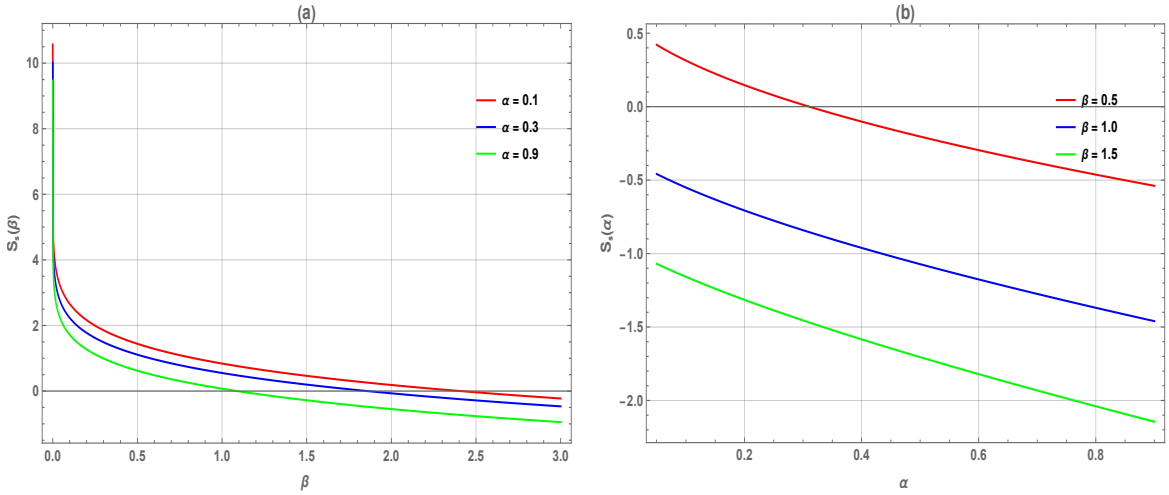

Figure 9: : (The left pane(a)), the superstatistic entropy S is displayed as a function of Inverse temperature parameter β for various values of α, and (The right panel(b), is displayed as a function of α, for various values of deformed parameter β.

In the Fig.10(a) and (b) display the variation of the superstatistic Helmholtz free energy F_s with respect to the inverse temperature β and the deformation parameter α. In Fig10(a), F_s decreases nonlinearly as β increases, becoming more negative, which is consistent with the system approaching its ground state energy at low temperatures. The rate of this decline is greater for lower values of α, indicating a stronger thermodynamic response in less deformed systems. In Fig.10(b), $F_s(\alpha)$ increases smoothly with α, particularly at higher β, showing that deformation tends to reduce the thermodynamic cost of maintaining equilibrium. The results highlight that deformation not only modifies the energy spectrum but also stabilizes the system thermodynamically. Overall, α softens the temperature dependence of free energy, acting as a structural regulator of equilibrium properties.

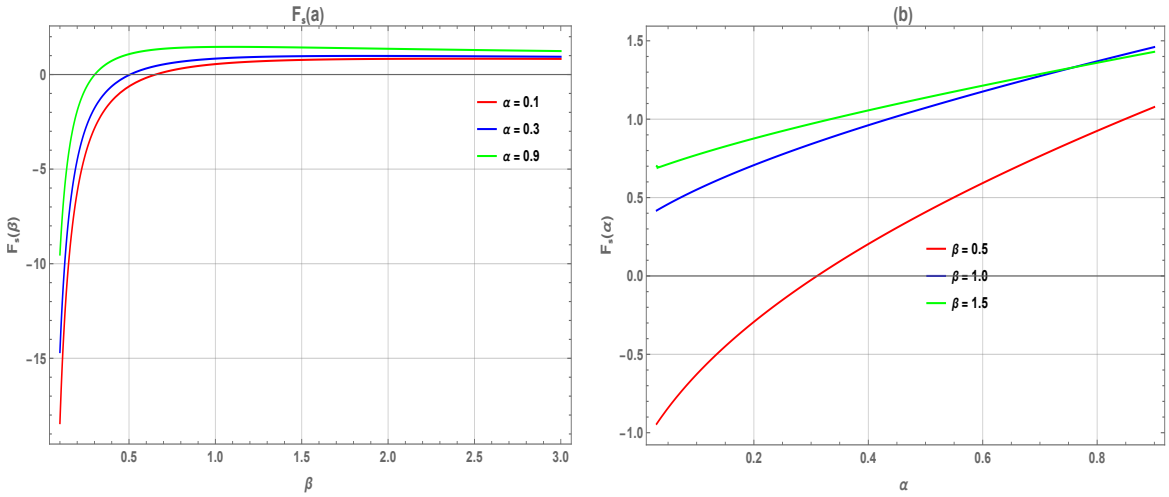

Figure 10: : (The left panel(a), the superstatistic free energy F is displayed for various values of α as a function of Inverse temperature parameter β, and (The right panel(b), is displayed as a function of α, for various values of deformed parameter β.

In the Fig.11(a) , $C_s(\beta)$ shows a smooth increase with the inverse temperature parameter β, saturating at large β, which is consistent with thermodynamic behavior under superstatistical regimes. This trend indicates enhanced energy fluctuations at intermediate β, often associated with metastable or transition regions. In contrast, Fig.11(b) shows that $C_s(\alpha)$ decreases monotonically with increasing position-dependent mass parameter α, for all fixed values of β. This behavior suggests that greater spatial variation in mass inhibits thermal excitations, thus lowering the specific heat. These observations are consistent with prior studies on systems governed by position-dependent mass and generalized coherent states, where both temperature and mass modulation significantly influence thermal response and statistical properties.

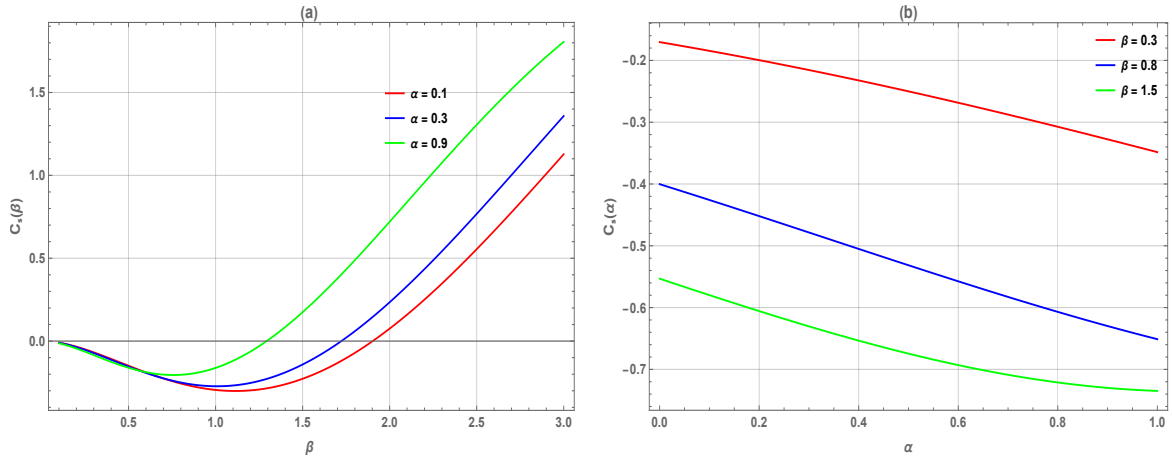

Figure 11: (The left panel(a), the superstatistic specific heat C_s is displayed as a function of for various values of Inverse temperature parameter β, and (The right panel(b), is displayed as a function of C_s, for various values of α for fixed deformed parameter β.

5 Conclusion

This work explores the thermodynamic and superstatistical properties of a harmonic oscillator with a position-dependent mass (PDM) under a quadratic deformation governed by a parameter α. By solving the deformed Schrödinger equation analytically, the authors derive energy spectra and Gazeau–Klauder coherent states, which are then used to compute thermodynamic quantities such as partition function $Z(\beta)$, mean energy $U(\beta)$, entropy $S(\beta)$, heat capacity $C(\beta)$, and free energy $F(\beta)$. The numerical analysis reveals that the deformation parameter α plays a key role in modulating thermal behavior: increasing α reduces entropy and specific heat, indicating stronger confinement and fewer accessible microstates. The results also show smooth, monotonic trends in all thermodynamic functions, suggesting the absence of critical behavior. Moreover, the superstatistical framework enhances the understanding of thermal fluctuations in systems with inhomogeneous structures, showing that α can be used as a tunable parameter to control quantum thermodynamic responses. These insights contribute meaningfully to the theoretical modeling of nanoscale systems and coherent quantum states in deformed environments.

Disclaimer (Artificial intelligence)
Option 1:
Author(s) hereby declare that NO generative AI technologies such as Large Language Models (ChatGPT, COPILOT, etc.) and text-to-image generators have been used during the writing or editing of this manuscript.
Option 2:
Author(s) hereby declare that generative AI technologies such as Large Language Models, etc. have been used during the writing or editing of manuscripts. This explanation will include the name, version, model, and source of the generative AI technology and as well as all input prompts provided to the generative AI technology
Details of the AI usage are given below:
1.
2.
3.

Acknowledgments

We acknowledges LMT for useful discussions.

References

[1] L. Lawson, K. Amouzouvi, K. Sodoga, K. Beltako, Position-dependent mass from noncommutativity and its statistical descriptions, IJGMP, 21, 2450137 (2024).

[2] Ikot, A. N., Okon, I. B., Okorie, U. S., Omugbe, E., Abdel-Aty, A., Obagboye, L. F., ... and Qadir, K. W. (2023). Exact solutions of position dependent mass schrodinger equation with pseudoharmonic oscillator and its thermal properties using extended nikiforov-uvarov method.. https://doi.org/10.21203/rs.3.rs-2659340/v1.

[3] R. Costa Filho et al., "Position-dependent mass harmonic oscillator and deformed space," J. Math. Phys. 59, 042101 (2018) https://doi.org/10.1063/1.5020225.

[4] G. Bastard, Wave Mechanics Applied to Semiconductors, Les Editions de Physique, CNRS (1988).

[5] O. Von Roos, H. Mavromatis, Position-dependent effective masses in semiconductor theory. II, Phys. Rev. B 31 (1985) 2294.

[6] L.I. Serra and E. Lipparini, Spin response of unpolarized quantum dots, Europhys. Lett 40, 667 (1997).

[7] P. Harrison, Quantum Wells, Wires and Dots : Quantum Wells, Wires and Dots: Theoretical and Computational Physics of Semiconductor Nanostructures (John Wiley and Sons, 2000).

[8] L. Smith and C. Mailhiot, Theory of semiconductor superlattice electronic structure, Rev. Mod. Phys. **62**, 173 (1990).

[9] O. Von Roos, Position-dependent effective masses in semiconductor theory,Phys. Rev. B27 (1983) 7547.

[10] R.A. Morrow, Establishment of an effective-mass Hamiltonian for abrupt heterojunctions, Phys. Rev. B35 (1987), 074.

[11] W. Trzeciakowski and M. Gurioli, Electric-field effects in semiconductor quantum wells,Phys. Rev. B, 44(1991)3880.

[12] A. Schulze-Halberg, "Darboux Transformations for Effective Mass Schrodinger Equations with Energy-Dependent Potentials," International Journal of Modern Physics A, Vol. 23, No. 3-4, 2008, p. 537. doi:10.1142/S0217751X0803807X.

[13] C. Tezcan and R. Sever, A General Approach for the Exact Solution of the Schrödinger Equation, J. Math. Chem. 42(2007) 387.

[14] S. Meyur, S. Maji, S. Debnath, Analytical Solution of the Schrödinger Equation with Spatially Varying Effective Mass for Generalised Hylleraas Potential, Adv. High Ener. Phys. (7) (2014) ID952597.

[15] B. Gonul, B. Gonul, D. Tutco, O. Ozer, Supersymmetric Approach to Exactly Solvable Systems with Position-Dependent Effective Masses, Mod. Phys. Lett. A17 (2002) 2057.

[16] C. Quesne, B. Bagchi, A. Banergee and V. M. Tkachuk, Hamiltonians with Position-Dependent Mass, Deforma- tions and Supersymmetry,Bul. J. Phys. 33 (2006) 308.

[17] J.J. Pena, J. Morales, E. Zamora-Gallardo, J. García-Ravelo, Exactly solvable Schrödinger equations with a position-dependent mass: Null potential, Int. J. Quant. Chem. 100 (2004) 957.

[18] S.C.Y. Cruz, O. Rosas-Ortiz,Position Dependent Mass Oscillators and Coherent States, J. Phys. Math. Theor. 42 (2009) 185205.

[19] J. Yu, S.-H. Dong, Exactly solvable potentials for the Schrödinger equation with spatially dependent mass, Phys. Lett. A 325 (2004) 194.

[20] L. Lawson, Position-dependent mass in strong quantum gravitational background fields, J. Phys. A: Math. Theor. 55, 105303 (2022).

[21] L. Lawson, Minimal and maximal lengths of quantum gravity from non-hermitian position-dependent noncommutativity, Scientific Reports **12**, 20650 (2022).

[22] L. Lawson, P. Osei, Gazeau-Klauder coherent states in position-deformed Heisenberg algebra, Journal of Physics Communications, 6, 085016 (2022).

[23] R. Costa Filho, M. Almeida, G. Farias, J. Andrade,Displacement operator for quantum systems with position-dependent mass, Phys. Rev. A 84, 050102 (2011).

[24] K. Ullah, H. Ullah, Enhanced optomechanically induced transparency and slow/fast light in a position-dependent mass optomechanics, Eur. Phys. J. D , 74, 197 (2020).

[25] S. Mazharimousavi,Revisiting the displacement operator for quantum systems with position-dependent mass, Phys Rev A, 85, 034102 (2012).

[26] N. Amir and S. Iqba,Coherent states of position-dependent mass trapped in an infinite square well, J. Math. Phys. 61, 082102 (2020).

[27] G. Bruno da Costa and Ernesto P. Borges, A position-dependent mass harmonic oscillator and deformed space , J. Math. Phys. 59, 042101 (2018).

[28] M. Rego-Monteiro and F. Nobre,Classical field theory for a non-Hermitian Schrödinger equation with position-dependent masses, Phys Rev A 88 88, 032105 (2013).

[29] Ikot, A.N., Okon, I.B., Okorie, U.S. et al. Exact solutions of position-dependent mass Schrödinger equation with pseudoharmonic oscillator and its thermal properties using extended Nikiforov–Uvarov method. Z. Angew. Math. Phys. 75, 18 (2024). https://doi.org/10.1007/s00033-023-02150-2.

[30] R. Khordad. Thermodynamical properties of triangular quantum wires: entropy, specific heat, and internal energy. Continuum Mech. Thermodyn. DOI 10.1007/s00161-015-0429-2 .

[31] S. H.Dong ,W.H. Huang, P. Sedaghatnia and J. Hassanabadi, Exact solutions to generalized Dunkl oscillator and its thermodynamic properties, Res. Phys. 34 (2022) 105294.

[32] E. P. Inyang, E. S. William, E. Omugbe, E. P. Inyang, E. A. Ibanga, F. Ayedun, I. O. Akpan, and J. E. Ntibi. Application of Eckart-Hellmann potential to study selected diatomicmolecules using Nikiforov-Uvarov-Functional analysis method. Revista Mexicana de Fısica 68 (2022) 020401.

[33] S. Iqbal, Quantum Dynamical Recurrences in Position-Dependent Mass Systems, J. Rus. Laser Res.43(2022)96.

[34] R.A. El-Nabulsi, A new approach to the schrodinger equation with position-dependent mass and its implications in quantum dots and semiconductors, J. Phys.and Chem. Solids, 140 (2020) 109384.

[35] Amir Naila and Iqbal Shahid, Exact Solutions of Schrödinger Equation for the Position-Dependent Effective Mass Harmonic Oscillator, Commun. Theor. Phys. (2014) 62 790.

[36] Daniel Sabi Takou and Assimiou Yarou Mora and Ibrahim Nonkané and Latévi M. Lawson and Gabriel Y. H. Avossevou,Gazeau-Klauder coherent states for a harmonic position-dependent mass, eprint:2503.23043 arXiv quant-ph https://arxiv.org/abs/2503.23043.

[37] S. Sargolzaeipor et al., "q-deformed superstatistics in commutative and noncommutative spaces," EPJ Plus 133 (2018)

[38] Ikot, A.N. et al.,Superstatistics of Schrödinger equation with pseudo-harmonic potential in external magnetic and Aharanov-Bohm fields, Heliyon, Volume 6, Issue 4, e03738

[39] Ignacio S. Gomez, Matheus G. A. Santos, Daniela de Almeida dos Santos and Ronaldo Thibes, Partition function for position-dependent mass systems from superestatistics, https://doi.org/10.48550/arXiv.2503.16748, (2025).

[40] Uduakobong S. Okorie, Akpan N. Ikot, Ituen B. Okon, Lewis F. Obagboye, Ridha Horchani , Hewa Y. Abdullah 6, Karwan W. Qadir 7 and Abdel Haleem Abdel Aty, Exact solutions of κ dependent Schrödinger equation with quantum pseudo harmonic oscillator and its applications for the thermodynamic properties in normal and superstatistics https://doi.org/10.1038/s41598-023-28973-7 (Publié dans Scientific Reports, 2023).

[41] Omar Mustafa and S. Habib Mazharimousavi, A singular position-dependent mass particle in an infinite potential well, Physics Letters A, 373 (2008) 325-327 https://api.semanticscholar.org/CorpusID:18033453.

[42] H. Hassanabadi and M. Hosseinpoura, Thermodynamic properties of neutral particle in the presence of topological defects in magnetic cosmic string background. Eur. Phys. J. C 76 (2016) 553.

[43] X-L. Peng, R. Jiang, C-S. Jia, L-H. Zhang and Y-L. Zhao. Gibbs free energy of gaseous phosphorus dimer. Chem. Engr. Science 190 (2018) 122.

[44] C-S. Jia, C-W. Wang, L-H. Zhang, X-L. Peng, R. Zeng and X-T. You. Partition function of improved Tietz oscillators. Chem. Phys. Lett. 676 (2017) 150.

[45] C-S. Jia, L-H. Zhang, X-L. Peng, J-X. Luo, Y-L. Zhao, J-Y. Liu, J-J. Guo and L-D. Tang, Prediction of entropy and Gibbs free energy for nitrogen, Chemical Engineering Science 202 (2019) 70–74.

[46] R. Jiang, C-S. Jia, Y-Q. Wang, X-L. Peng and L-H. Zhang, Prediction of Gibbs free energy for the gases Cl2, Br2, and HCl. Chemical Physics Letters 726 (2019) 83-86.

[47] C. Beck, Superstatistics: theory and application, Contin. Mech. Thermod. 16, 293, (2004).

[48] C. Beck, "Superstatistics: theory and applications," Continuum Mechanics and Thermodynamics, vol. 16, no. 3, pp. 293–304, 2004.

[49] C. O. Edet, P. O. Amadi, U. S. Okorie, A. Tas, A. N. Ikot, and G. Rampho, Superstatistics of Schrödinger equation with pseudo-harmonic potential in external magnetic and Aharanov-Bohm fields, Revis. Mexic. de fisca. 66, 824, (2020).

[50] C. Beck and E. G. Cohen, "Superstatistics," Physica A, vol. 322, pp. 267–275, 2003.

[51] A.N. Ikot ,U.S. Okorie, G. Osobonye,P.O. Amadi ,C.O. Edet, M.J. Sithole, G.J. Rampho , Superstatistics of Schrödinger equation with pseudo-harmonic potential in external magnetic and Aharanov-Bohm fields,R. Sever, Heliyon 6 (2020) e03738 .

[52] C. O. Edet, P. O. Amadi, U. S. Okorie, A. Tas, A. N. Ikot, and G. Rampho, "Solutions of Schrodinger equation and thermal properties of generalized trigonometric Poschl-Teller potential," Revista Mexicana defisca, vol. 66, pp. 824–839, 2020.

[53] S. Sargolzaeipor, H. Hassanabadi,W.S. Chung, q-deformed superstatistics of the Schrödinger equation in commutative and noncommutative spaces with magnetic field, Eur. Phys. J. Plus 133 (2018)5.